

Solid Electrolytes in the Spotlight



Cite This: *Chem. Mater.* 2022, 34, 463–467



Read Online

ACCESS |

Metrics & More

Article Recommendations

This virtual issue is targeted to students and researchers, and highlights 32 research articles published over the past 5 years (from July 2016 to July 2021) in *Chemistry of Materials* (CM). The compilation of papers summarizes the latest advances in the field of solid-state electrolytes for lithium (Li)-, sodium (Na)-, and multivalent-ion (not among the 32 articles discussed) all-solid-state batteries (ASSBs), with a focus on inorganic materials and excluding hybrid systems, e.g., polymer/ceramic composites or systems including liquid media. A total of 125 articles reporting exciting experimental and/or theoretical findings on solid electrolytes were considered for this issue. During 2017–2019, there were about 25–30 papers published per year on this topic, but 2020 and 2021 saw a significant increase, with 26 publications in the first half of 2021 alone. Submissions came from many countries around the world, as shown in Figure 1. While most papers were led by research groups located in the United States, Germany and Japan follow closely, and Austria, the United Kingdom, Canada, and China are also well represented.

By far the largest number of CM articles concern solid-state electrolytes for Li-ion battery applications (94 papers), with Na-ion conductors (25 papers) a distant second. Electrolytes for multivalent systems (Mg^{2+} , Ca^{2+} , and Zn^{2+}) and fluoride ion conductors remain niche topics (6 papers).

Sulfide-based solid electrolytes have been under intense scrutiny as many demonstrate remarkably high ionic conductivities at room temperature (some even higher than that of common liquid electrolytic solutions) and can be prepared in dense pellets without the need for sintering. Nonetheless, most sulfide electrolytes are unstable in air and/or suffer from poor anodic and cathodic stabilities, which may hinder their practical application. While 54 papers have been published on Li-ion conducting sulfides, Na-based sulfides and their applications in Na ASSBs have also received significant attention.^{1–6} Through a multitechnique approach, including Raman spectroscopy, pair-distribution function analysis, inelastic neutron scattering, density functional theory (DFT), X-ray diffractions (XRD), and differential scanning calorimetry, Famprikis and collaborators⁴ have disentangled the much debated crystal symmetry of the high-conductivity “cubic”- Na_3PS_4 phases and the second-order phase-transition tetragonal-to-cubic, which is responsible for the material’s high ionic conductivities ($\sim 10^{-4}$ S/cm). Raman spectroscopy was crucial to observing that the “cubic”- Na_3PS_4 phases contain remnants of tetragonal character,⁴ which aids Na-ion transport at higher temperatures. This study emphasizes that the usual combination of powder XRD and electrochemical impedance spectroscopy (EIS) alone is not sufficient to reveal the complex interplay of structure and ionic conductivity in solid electro-

lytes. Other chalcogenide solid electrolytes, $Na_{11}Sn_2XS_{12}$ or $Na_{11}Sn_2XSe_{12}$ (with X = P and Sb), have demonstrated impressive Na-ion conductivities (1–4 mS/cm)^{5,6} but are unstable in the presence of oxygen and moisture. Based on the idea that “soft acid” sulfides are more stable under ambient conditions, Ramos et al.⁵ developed an antimony-based $Na_{11}Sn_2SbS_{12}$ analogue, with good structural stability and a marginal decrease in Na-ion conductivity after being exposed to dry air for 36 h.

Among the novel and rediscovered solid electrolyte chemistries, oxy/hydroxyhalides and halides have shown particular promise. Oxy/hydroxyhalides with the antiperovskite structure offer high ionic conductivities on the order of mS/cm. Li-rich antiperovskites (e.g., $Li_{3-x}(OH_x)Cl$) are of interest due to their low cost, but their synthesis requires stringent conditions and their exact composition, structure, and ion conduction mechanism remain unclear. Hanghofer et al.⁷ have examined a range of Li–OH–Cl antiperovskites using neutron diffraction and NMR. They reported the first structural models for the cubic phase and a new orthorhombic phase, which also contained structural information about the H atoms in the framework. Their work indicates that $Li_4(OH)_3Cl$ and variants of $Li_{3-x}(OH_x)Cl$, where $x > 0$, are the only stable Li-rich antiperovskites.⁷ Using complementary experimental and computational methods, Wang and collaborators have shown that the high Li-ion conductivity in Li_2OHCl is correlated to the “paddlewheel” rotation of the OH^- anions.⁸

Rocksalt-type lithium ternary halide electrolytes (with general formula Li_3MX_6) have also attracted significant attention over the past few years. A computational study of the phase and electrochemical stability by Yu and co-workers has predicted that chlorides have the highest oxidation potential (~ 4.3 V vs Li/Li⁺) and elastic moduli within this class of materials, making them particularly compatible with high-voltage cathodes.⁹ Additionally, aliovalent substitution of M^{3+} for Zr^{4+} is expected to enhance Li-ion conduction, resulting in low diffusion barriers (~ 0.25 eV). These predictions have been confirmed by Helm et al.,¹⁰ who explored the series of $Li_{3-x}In_{1-x}Zr_xCl_6$ electrolytes and demonstrated, using high-resolution diffraction data, the presence of a new tetrahedrally coordinated Li position

Published: January 25, 2022



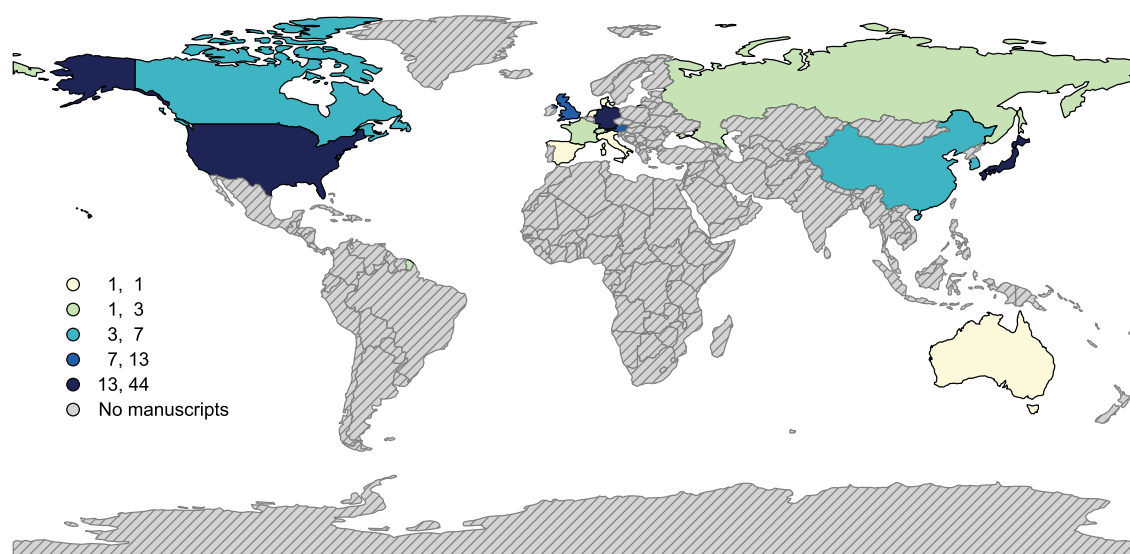


Figure 1. Global distribution of research activities on all-solid-state electrolytes published in CM over the past 5 years. Gray hatched areas show countries without publications on this topic in CM.

together with cation disorder. These structural features together with the increase in the number of vacancies led to the formation of a 3D Li-ion diffusion network and increased room temperature Li-ion conductivity.

The development of design rules for solid electrolytes hinges on an understanding of the electrolyte composition, structure, and microstructure and how these affect the conduction of ions, the mechanical properties, and the thermal and electrochemical stabilities toward electrode materials. Besides diffraction techniques, solid-state NMR (SS-NMR) has emerged as an important tool to investigate the local structure of solid electrolytes and provides quantitative information on both crystalline and amorphous phases present in the sample. Using SS-NMR, Harm et al. identified a low conductivity amorphous thiophosphate phase with low Si content in tetragonal Li_7SiPS_8 ,¹¹ a new member of the $\text{Li}_{10}\text{GeP}_2\text{S}_{12}$ (LGPS)-type family. This impurity resulted in limited intergranular conductivity, explaining the unexpectedly low bulk conductivity observed with EIS. This case study highlights the need for comprehensive structural analysis of glass-ceramic compounds beyond the crystalline fractions.¹¹ SS-NMR is also an indispensable tool for the characterization of chalcogenide glasses, as exemplified by Marple and co-workers for the study of the $\text{Li}_2\text{S}-\text{Ga}_2\text{Se}_3-\text{GeSe}_2$ family of compounds.¹²

The study by Wang et al.⁸ emphasized the role of anion rotations in the mechanism of Li-ion conduction in the antiperovskite Li_2OHCl electrolyte. Variable-temperature X-ray and neutron diffraction experiments and EIS were essential for correlating an orthorhombic to cubic phase transition with an ~ 100 -fold increase in ionic conductivity near 311 K. Furthermore, quasi-elastic neutron scattering, maximum entropy method analysis of the neutron diffraction data, and *ab initio* molecular dynamics simulations (AIMD) together correlated fast Li-ion diffusion with the local rotations of framework OH^- anions. This work illustrates the power of combining experimental and computational tools to probe dynamic processes over a range of lengths and time scales. By far the most commonly used tool for probing bulk ionic conductivity is EIS; here, we recommend a Methods/Protocols article by Krasnikova et al.¹³ that proposes a unified approach

toward obtaining reliable EIS data on ion-conducting ceramics, verifying the equivalent circuit by adjusting the temperature, and estimating errors in measurements.

The identification of electrolyte degradation pathways during handling and processing is key to the development of effective manufacturing protocols. Using a combination of *operando* optical microscopy, Raman spectroscopy, synchrotron XRD, and *in situ* XANES, Sun and co-workers showed that rocksalt-type Li_3InCl_6 reacts with water upon air exposure, which reduces drastically its ionic conductivity.¹⁴ While In_2O_3 , LiCl , and HCl formed at the surface of the particles upon reaction with adsorbed water, H_2O molecules inserted into the particles and led to $\text{Li}_3\text{InCl}_6 \cdot x\text{H}_2\text{O}$ hydrates. Likewise, Sharafi et al.¹⁵ and Brugge et al.¹⁶ using X-ray photoelectron spectroscopy (XPS) have demonstrated that $\text{Li}_7\text{La}_3\text{Zr}_2\text{O}_{12}$ (LLZO) reacts vigorously with CO_2 and H_2O at ambient conditions, with significant effects on the solid electrolyte ionic conductivity.

An understanding of the practical electrochemical stability of solid electrolytes and their (electro)chemical reactivity against electrode materials is key to identifying viable electrode/electrolyte combinations to engineer ASSBs. Yet, the presence of buried interfaces in fully assembled devices complicates diagnosis, requiring the implementation of specialized tools that can provide spatially resolved information on interfacial compounds present in minute concentrations. *Ex situ* inspection of half cells allows longer data acquisition times and larger sample volumes to compensate for sensitivity limitations. Auvergniot and collaborators elegantly used X-ray photoelectron and Auger spectroscopies to monitor the degradation of buried interfaces formed between $\text{Li}_6\text{PS}_5\text{Cl}$ and three commercial cathodes LiCoO_2 , $\text{LiNi}_{1/3}\text{Co}_{1/3}\text{Mn}_{1/3}\text{O}_2$, and LiMn_2O_4 .¹⁷ They isolated the oxidation products of $\text{Li}_6\text{PS}_5\text{Cl}$, namely, LiCl , phosphate species, lithium polysulfides, and elemental sulfur. In the same vein, Walther et al.¹⁸ demonstrated that time-of-flight secondary-ion mass spectrometry (ToF-SIMS) and XPS provide valuable insights into interphase compositions and their microstructures in ASSBs, including the local structure and morphology of the reaction layer between the cathode ($\text{LiNi}_{0.6}\text{Co}_{0.2}\text{Mn}_{0.2}\text{O}_2$) and the solid

electrolyte ($\text{Li}_6\text{PS}_5\text{Cl}$). Remarkably, Hakari et al.¹⁹ have circumvented sensitivity issues by preparing “magnified interfaces” consisting of a composite electrode of Li_3PS_4 glass electrolyte and carbon. This composite increased the contact area with the Li metal electrode and facilitated the *ex situ* observation of electrochemical reactions and decomposition. Interfacial reactions have also been studied as a function of temperature using surface-sensitive synchrotron X-ray absorption spectroscopy and a thin film composite cathode consisting of LLZO and $\text{LiNi}_{0.6}\text{Co}_{0.2}\text{Mn}_{0.2}\text{O}_2$ to elucidate the interfacial reactions that occur during co-sintering in typical electrode fabrication processes.²⁰ Using a related model system and ToF-SIMS, Park et al.²¹ observed compositional changes at the LLZO/ LiCoO_2 interface resulting from cross-exchange of La and Co at the interface, which could be mitigated with a Li_3BO_3 surface coating.

When it comes to *in situ* and *operando* investigations, sensitivity limitations are aggravated by the constraints imposed by full device analysis, yet several studies have provided new and important insights into key degradation processes. For example, Sang et al. examined the reactions of LGPS and Li_3PS_4 with Li metal using *in situ* and *operando* Raman and identified the reversible reduction of $\text{P(V)}\text{S}_4^{3-}$ moieties into $\text{P(IV)}_2\text{S}_6^{4-}$ units.²² The inherent challenges in probing interfaces through experimental methods have stimulated significant efforts in the modeling area.²³ Relying on the power of DFT and AIMD simulations, a robust thermodynamic framework, and database science, Tang et al.²³ have developed a multitier approach to investigate the chemical, electrochemical, and kinetic evolution of interfaces in ASSBs. For instance, pair distribution functions derived from AIMD simulations fingerprinted on a library of binary compounds showed that the decomposition of the $\text{NaCoO}_2/\text{Na}_3\text{PS}_4$ interface gives rise to the formation of sulfate groups and Na_3P compounds.

Understanding and mitigating the formation of Li dendrites during cycling is an important step toward the deployment of high energy density ASSBs based on a Li metal anode. Despite the high bulk modulus of ceramic electrolytes, Li dendrites have been found to form within grain boundaries, resulting in cell shorts upon extended cycling. Using ^7Li chemical shift imaging and electron microscopy, Marbella et al.²⁴ monitored Li microstructural growth during galvanostatic cycling of $\text{Li}_{6.5}\text{La}_3\text{Zr}_{1.5}\text{Ta}_{0.5}\text{O}_{12}$ and correlated their findings with alterations in the voltage profiles. This study showed that magnetic resonance imaging enables the detection of Li microstructures well before short-circuits. Additionally, transformations of both the stripping and the plating interfaces were observed, indicating heterogeneities in both Li removal and deposition. While smooth Li electroplating has been the focus of strategies to mitigate Li dendrites, recently, a DFT and kinetic Monte Carlo study by Yang and co-workers showed that the Li stripping process is equally critical to the formation of the Li microstructure.²⁵ The authors showed that the nature of the solid electrolyte interphases at the surface of the Li metal anode played an important role in the formation of nonuniform local current densities and dendrite nucleation, suggesting that electrode coating strategies can be effective for maintaining a smooth Li surface during the stripping process.

In closing, step advances in the field rely on the identification and synthesis of new and improved ion conductors. One traditional approach is through elemental

substitution to determine the solid solution range and the impact on ionic conductivity. For instance, NaSiCONs (sodium superionic conductors) with general formula $\text{Na}_{1+x}\text{Zr}_2\text{Si}_x\text{P}_{3-x}\text{O}_{12}$ ($0 \leq x \leq 3$) form the basis of many Na-ion solid electrolytes (but also Li-ion).²⁶ Ma et al.²⁷ and later Deng et al.²⁸ have explored the partial substitution of zirconium by scandium over a large range of compositions in the NaSiCON $\text{Na}_{3+x}\text{Sc}_x\text{Zr}_{2-x}\text{Si}_2\text{PO}_{12}$ structure using a scalable solution-assisted solid-state reaction method. In this case, solid solutions were obtained for all compositions, and the highest room temperature conductivity of 4.0×10^{-3} S/cm was achieved for the $x = 0.4$ sample.²⁷

High-throughput experimental and theoretical screening approaches have been used to accelerate the identification of promising conductors and their synthesizabilities. A combinatorial approach was recently employed to explore the Li–La–Ti–O pseudoternary phase diagram,²⁹ with over 576 samples synthesized and characterized by XRD. While perovskite LLTOs can be obtained over a wide compositional range, they are never phase-pure but coexist with secondary phases, such as TiO_2 . Recently, a guided search for fast ion conductors was carried out using a machine learning-based prediction model for materials selection.³⁰ DFT-MD simulations were then used to calculate ionic conductivity. Over 12 000 materials were screened, and several new solid materials with predicted superionic lithium conduction were identified. Notably, $\text{Li}_5\text{B}_7\text{S}_{13}$ has a predicted room temperature Li-ion conductivity of ~ 74 mS/cm, several times higher than those of the best-known ion conductors to date.

While the intragrain conductivity is largely determined by the crystal structure, sample density and microstructure strongly influence the macroscopic conductivity and must be controlled during synthesis. *Operando* synchrotron XRD and mesoscale modeling were recently used to understand the effects of calcination and densification on LLZO.³¹ This study found that the most effective densification is obtained when small and bimodal distributions of particles are used. Grain boundary contributions to ionic transport in LLZO were computationally examined by Yu et al.³² Specifically, the energetics, composition, and transport properties of several low energy symmetric tilt grain boundaries in LLZO were characterized at the atomic scale. While lithium transport is generally reduced in grain boundaries, the magnitude of this effect depends on temperature and grain boundary structure, in keeping with experimental findings.

Research in solid electrolytes and their batteries is exciting, fast-paced, and multidisciplinary. New synthesis strategies, specialized *in situ* and *operando* characterization measurements, and computational techniques to probe unique phenomena of ASSBs are being developed. The development of working ASSBs certainly requires new insights, which may be achieved through knowledge transfer from other areas of material science, such as solid oxide fuel cells, semiconductor technologies, functional polymers, metallurgy, and others.

Marca M. Doeff  orcid.org/0000-0002-2148-8047

Raphaële J. Clément  orcid.org/0000-0002-3611-1162

Pieremanuele Canepa  orcid.org/0000-0002-5168-9253

■ AUTHOR INFORMATION

Complete contact information is available at:

<https://pubs.acs.org/10.1021/acs.chemmater.1c03770>

Notes

Views expressed in this editorial are those of the authors and not necessarily the views of the ACS.

RELATED READINGS

(1) de Klerk, N. J. J.; Rosloń, I.; Wagemaker, M. Diffusion Mechanism of Li Argyrodite Solid Electrolytes for Li-Ion Batteries and Prediction of Optimized Halogen Doping: The Effect of Li Vacancies, Halogens, and Halogen Disorder. *Chem. Mater.* **2016**, *28*, 7955–7963.

(2) Weber, D. A.; Senyshyn, A.; Weldert, K. S.; Wenzel, S.; Zhang, W.; Kaiser, R.; Berendts, S.; Janek, J.; Zeier, W. G. Structural Insights and 3D Diffusion Pathways within the Lithium Superionic Conductor $\text{Li}_{10}\text{GeP}_2\text{S}_{12}$. *Chem. Mater.* **2016**, *28*, 5905–5915.

(3) Suzuki, N.; Richards, W. D.; Wang, Y.; Miara, L. J.; Kim, J. C.; Jung, I.-S.; Tsujimura, T.; Ceder, G. Synthesis and Electrochemical Properties of $\bar{I}4$ -Type $\text{Li}_{1+2x}\text{Zn}_{1-x}\text{PS}_4$ Solid Electrolyte. *Chem. Mater.* **2018**, *30*, 2236–2244.

(4) Famprakis, T.; Bouyanff, H.; Canepa, P.; Zbiri, M.; Dawson, J. A.; Suard, E.; Fauth, F.; Playford, H. Y.; Dambournet, D.; Borkiewicz, O. J.; Courty, M.; Clemens, O.; Chotard, J.-N.; Islam, M. S.; Masquelier, C. Insights into the Rich Polymorphism of the Na^+ Ion Conductor Na_3PS_4 from the Perspective of Variable-Temperature Diffraction and Spectroscopy. *Chem. Mater.* **2021**, *33*, 5652–5667.

(5) Ramos, E. P.; Zhang, Z.; Assoud, A.; Kaup, K.; Lalère, F.; Nazari, L. F. Correlating Ion Mobility and Single Crystal Structure in Sodium-Ion Chalcogenide-Based Solid State Fast Ion Conductors: $\text{Na}_{11}\text{Sn}_2\text{PnS}_{12}$ (Pn = Sb, P). *Chem. Mater.* **2018**, *30*, 7413–7417.

(6) Duchardt, M.; Neuberger, S.; Ruschewitz, U.; Krauskopf, T.; Zeier, W. G.; Schmedt auf der Günne, J.; Adams, S.; Roling, B.; Dehnen, S. Superior Conductor $\text{Na}_{11.1}\text{Sn}_{2.1}\text{P}_{0.9}\text{Se}_{12}$: Lowering the Activation Barrier of Na^+ Conduction in Quaternary 1–4–5–6 Electrolytes. *Chem. Mater.* **2018**, *30*, 4134–4139.

(7) Hanghofer, I.; Redhammer, G. J.; Rohde, S.; Hanzu, I.; Senyshyn, A.; Wilkening, H. M. R.; Rettenwander, D. Untangling the Structure and Dynamics of Lithium-Rich Anti-Perovskites Envisaged as Solid Electrolytes for Batteries. *Chem. Mater.* **2018**, *30*, 8134–8144.

(8) Wang, F.; Evans, H. A.; Kim, K.; Yin, L.; Li, Y.; Tsai, P.-C.; Liu, J.; Lapidus, S. H.; Brown, C. M.; Siegel, D. J.; Chiang, Y.-M. Dynamics of Hydroxyl Anions Promotes Lithium Ion Conduction in Antiperovskite Li_2OHCl . *Chem. Mater.* **2020**, *32*, 8481–8491.

(9) Kim, K.; Park, D.; Jung, H.-G.; Chung, K. Y.; Shim, J. H.; Wood, B. C.; Yu, S. Material Design Strategy for Halide Solid Electrolytes Li_3MX_6 ($X = \text{Cl}, \text{Br}, \text{and I}$) for All-Solid-State High-Voltage Li-Ion Batteries. *Chem. Mater.* **2021**, *33*, 3669–3677.

(10) Helm, B.; Schlem, R.; Wankmiller, B.; Banik, A.; Gautam, A.; Ruhl, J.; Li, C.; Hansen, M. R.; Zeier, W. G. Exploring Aliovalent Substitutions in the Lithium Halide Superionic Conductor $\text{Li}_{3-x}\text{In}_{1-x}\text{Zr}_x\text{Cl}_6$ ($0 \leq x \leq 0.5$). *Chem. Mater.* **2021**, *33*, 4773–4782.

(11) Harm, S.; Hatz, A.-K.; Moudrakovski, I.; Eger, R.; Kuhn, A.; Hoch, C.; Lotsch, B. V. Lesson Learned from NMR: Characterization and Ionic Conductivity of LGPS-like Li_7SiPS_8 . *Chem. Mater.* **2019**, *31*, 1280–1288.

(12) Marple, M. A.; Aitken, B. G.; Kim, S.; Sen, S. Fast Li-Ion Dynamics in Stoichiometric $\text{Li}_2\text{S}-\text{Ga}_2\text{Se}_3-\text{GeS}_2$ Glasses. *Chem. Mater.* **2017**, *29*, 8704–8710.

(13) Krasnikova, I. V.; Pogosova, M. A.; Sanin, A. O.; Stevenson, K. J. Toward Standardization of Electrochemical Impedance Spectroscopy Studies of Li-Ion Conductive Ceramics. *Chem. Mater.* **2020**, *32*, 2232–2241.

(14) Li, W.; Liang, J.; Li, M.; Adair, K. R.; Li, X.; Hu, Y.; Xiao, Q.; Feng, R.; Li, R.; Zhang, L.; Lu, S.; Huang, H.; Zhao, S.; Sham, T.-K.; Sun, X. Unraveling the Origin of Moisture Stability of Halide Solid-State Electrolytes by *In Situ* and *Operando* Synchrotron X-Ray Analytical Techniques. *Chem. Mater.* **2020**, *32*, 7019–7027.

(15) Sharafi, A.; Kazyak, E.; Davis, A. L.; Yu, S.; Thompson, T.; Siegel, D. J.; Dasgupta, N. P.; Sakamoto, J. Surface Chemistry

Mechanism of Ultra-Low Interfacial Resistance in the Solid-State Electrolyte $\text{Li}_7\text{La}_3\text{Zr}_2\text{O}_{12}$. *Chem. Mater.* **2017**, *29*, 7961–7968.

(16) Brugge, R. H.; Hekselman, A. K. O.; Cavallaro, A.; Pesci, F. M.; Chater, R. J.; Kilner, J. A.; Agüero, A. Garnet Electrolytes for Solid State Batteries: Visualization of Moisture-Induced Chemical Degradation and Revealing Its Impact on the Li-Ion Dynamics. *Chem. Mater.* **2018**, *30*, 3704–3713.

(17) Auvergniot, J.; Cassel, A.; Ledeuil, J.-B.; Viallet, V.; Seznec, V.; Dedryvère, R. Interface Stability of Argyrodite $\text{Li}_6\text{PS}_5\text{Cl}$ toward LiCoO_2 , $\text{LiNi}_{1/3}\text{Co}_{1/3}\text{Mn}_{1/3}\text{O}_2$, and LiMn_2O_4 in Bulk All-Solid-State Batteries. *Chem. Mater.* **2017**, *29*, 3883–3890.

(18) Walther, F.; Koerver, R.; Fuchs, T.; Ohno, S.; Sann, J.; Rohnke, M.; Zeier, W. G.; Janek, J. Visualization of the Interfacial Decomposition of Composite Cathodes in Argyrodite-Based All-Solid-State Batteries Using Time-of-Flight Secondary-Ion Mass Spectrometry. *Chem. Mater.* **2019**, *31*, 3745–3755.

(19) Hakari, T.; Deguchi, M.; Mitsuhara, K.; Ohta, T.; Saito, K.; Orikasa, Y.; Uchimoto, Y.; Kowada, Y.; Hayashi, A.; Tatsumisago, M. Structural and Electronic-State Changes of a Sulfide Solid Electrolyte during the Li Deinsertion–Insertion Processes. *Chem. Mater.* **2017**, *29*, 4768–4774.

(20) Kim, Y.; Kim, D.; Bliem, R.; Vardar, G.; Waluyo, I.; Hunt, A.; Wright, J. T.; Katsoudas, J. P.; Yildiz, B. Thermally Driven Interfacial Degradation between $\text{Li}_7\text{La}_3\text{Zr}_2\text{O}_{12}$ Electrolyte and $\text{LiNi}_{0.6}\text{Mn}_{0.2}\text{Co}_{0.2}\text{O}_2$ Cathode. *Chem. Mater.* **2020**, *32*, 9531–9541.

(21) Park, K.; Yu, B.-C.; Jung, J.-W.; Li, Y.; Zhou, W.; Gao, H.; Son, S.; Goodenough, J. B. Electrochemical Nature of the Cathode Interface for a Solid-State Lithium-Ion Battery: Interface between LiCoO_2 and Garnet- $\text{Li}_7\text{La}_3\text{Zr}_2\text{O}_{12}$. *Chem. Mater.* **2016**, *28*, 8051–8059.

(22) Sang, L.; Haasch, R. T.; Gewirth, A. A.; Nuzzo, R. G. Evolution at the Solid Electrolyte/Gold Electrode Interface during Lithium Deposition and Stripping. *Chem. Mater.* **2017**, *29*, 3029–3037.

(23) Tang, H.; Deng, Z.; Lin, Z.; Wang, Z.; Chu, I.-H.; Chen, C.; Zhu, Z.; Zheng, C.; Ong, S. P. Probing Solid–Solid Interfacial Reactions in All-Solid-State Sodium-Ion Batteries with First-Principles Calculations. *Chem. Mater.* **2018**, *30*, 163–173.

(24) Marbella, L. E.; Zekoll, S.; Kasemchainan, J.; Emge, S. P.; Bruce, P. G.; Grey, C. P. ^7Li NMR Chemical Shift Imaging To Detect Microstructural Growth of Lithium in All-Solid-State Batteries. *Chem. Mater.* **2019**, *31*, 2762–2769.

(25) Yang, C.-T.; Qi, Y. Maintaining a Flat Li Surface during the Li Stripping Process via Interface Design. *Chem. Mater.* **2021**, *33*, 2814–2823.

(26) Deng, Z.; Sai Gautam, G.; Kolli, S. K.; Chotard, J.-N.; Cheetham, A. K.; Masquelier, C.; Canepa, P. Phase Behavior in Rhombohedral NaSiCON Electrolytes and Electrodes. *Chem. Mater.* **2020**, *32*, 7908–7920.

(27) Ma, Q.; Guin, M.; Naqash, S.; Tsai, C.-L.; Tietz, F.; Guillon, O. Scandium-Substituted $\text{Na}_3\text{Zr}_2(\text{SiO}_4)_2(\text{PO}_4)$ Prepared by a Solution-Assisted Solid-State Reaction Method as Sodium-Ion Conductors. *Chem. Mater.* **2016**, *28*, 4821–4828.

(28) Deng, Y.; Eames, C.; Nguyen, L. H. B.; Pecher, O.; Griffith, K. J.; Courty, M.; Fleutot, B.; Chotard, J.-N.; Grey, C. P.; Islam, M. S.; Masquelier, C. Crystal Structures, Local Atomic Environments, and Ion Diffusion Mechanisms of Scandium-Substituted Sodium Superionic Conductor (NASICON) Solid Electrolytes. *Chem. Mater.* **2018**, *30*, 2618–2630.

(29) Jonderian, A.; Ting, M.; McCalla, E. Metastability in Li–La–Ti–O Perovskite Materials and Its Impact on Ionic Conductivity. *Chem. Mater.* **2021**, *33*, 4792–4804.

(30) Sendek, A. D.; Cubuk, E. D.; Antoniuk, E. R.; Cheon, G.; Cui, Y.; Reed, E. J. Machine Learning-Assisted Discovery of Solid Li-Ion Conducting Materials. *Chem. Mater.* **2019**, *31*, 342–352.

(31) Barai, P.; Fister, T.; Liang, Y.; Libera, J.; Wolfman, M.; Wang, X.; Garcia, J.; Iddir, H.; Srinivasan, V. Investigating the Calcination and Sintering of $\text{Li}_7\text{La}_3\text{Zr}_2\text{O}_{12}$ (LLZO) Solid Electrolytes Using *Operando* Synchrotron X-Ray Characterization and Mesoscale Modeling. *Chem. Mater.* **2021**, *33*, 4337–4352.

(32) Yu, S.; Siegel, D. J. Grain Boundary Contributions to Li-Ion Transport in the Solid Electrolyte $\text{Li}_7\text{La}_3\text{Zr}_2\text{O}_{12}$ (LLZO). *Chem. Mater.* **2017**, *29*, 9639–9647.